

– Supporting information –

First-principles study of the voltage profile and mobility of Mg intercalation in a chromium oxide spinel

Tina Chen,^{†,‡} Gopalakrishnan Sai Gautam,^{§,‡} Wenxuan Huang,^{§,‡} and Gerbrand Ceder,^{†,‡}

[†]Department of Materials Science and Engineering, University of California, Berkeley,
California 94720, USA

[‡]Materials Science Division, Lawrence Berkeley National Lab, Berkeley, California 94720, USA

[§]Department of Materials Science and Engineering, Massachusetts Institute of Technology,
Cambridge, Massachusetts 02139, USA

1.1 ECI Information

Table S1: Cluster Expansion ECI information

Cluster No.	Cluster Type	Site in cluster			ECI	ECI/multiplicity
0	Empty	None			-150.8	-150.8
1	Point	0.625	0.125	0.125	61.6	30.8
2	Pair	0.625	0.125	0.125	18.2	4.5
		1.375	-0.125	-0.125		
3		0.625	0.125	0.125	106.3	8.9
		1.625	0.125	0.125		
4		0.625	0.125	0.125	-45.8	-3.8
	1.375	0.875	-0.125			
5	0.625	0.125	0.125	11.4	1.9	
	1.625	1.125	-0.875			
6	Triplet	0.625	0.125	0.125	-38.7	-3.2
		0.375	-0.125	-0.125		
		1.375	-0.125	-0.125		
7		0.625	0.125	0.125	7.3	0.9
		-0.375	0.125	0.125		
		-0.375	1.125	0.125		
8		0.625	0.125	0.125	12.3	0.3
		-0.625	-0.125	0.875		
		0.375	-0.125	1.875		
9		0.625	0.125	0.125	4.3	0.1
		-0.375	-0.875	1.125		
		0.625	-0.875	2.125		
10		0.625	0.125	0.125	-14.6	-0.3
		-0.375	0.125	0.125		
		1.375	0.875	-1.125		
11	0.625	0.125	0.125	11.6	0.5	
	-0.625	-0.125	0.875			
	-1.375	2.125	0.125			
12	0.625	0.125	0.125	13.0	1.1	
	-0.375	0.125	0.125			
	1.625	0.125	0.125			
13	0.625	0.125	0.125	-28.8	-0.6	
	0.375	-0.125	-0.125			
	2.625	0.125	-0.875			
14	0.625	0.125	0.125	-4.3	-0.2	
	-0.375	0.125	0.125			
	0.375	1.875	-2.125			
15	Quadruplet	0.625	0.125	0.125	-7.0	-0.6
		1.375	-0.125	-0.125		
		0.375	-0.125	-0.125		
		1.625	0.125	0.125		
16		0.625	0.125	0.125	7.6	0.2
		1.625	0.125	0.125		
		1.625	-0.875	0.125		
		2.375	-0.125	-0.125		
17		0.625	0.125	0.125	-7.6	-0.3
		1.375	-0.125	-0.125		
		0.375	-0.125	-0.125		
		1.625	0.125	-1.875		
	0.625	0.125	0.125			

18	1.625	0.125	0.125	11.2	1.4
	0.625	0.125	1.125		
	1.625	-1.875	1.125		
19	0.625	0.125	0.125	11.2	0.2
	1.375	-0.125	-0.125		
	0.375	-0.125	-0.125		
	1.375	0.875	-0.125		
20	0.625	0.125	0.125	-11.9	-0.5
	1.375	-0.125	-0.125		
	0.375	-1.125	0.875		
	2.375	-1.125	-0.125		
21	0.625	0.125	0.125	13.9	0.3
	1.625	0.125	0.125		
	1.375	-1.125	-0.125		
	2.375	-0.125	-0.125		
22	0.625	0.125	0.125	22.5	0.5
	1.375	-0.125	-0.125		
	0.625	-0.875	0.125		
	0.375	-1.125	-0.125		
23	0.625	0.125	0.125	-15.6	-0.3
	1.375	0.875	-0.125		
	-0.625	0.875	0.875		
	0.625	1.125	1.125		
24	0.625	0.125	0.125	10.5	0.4
	1.375	-0.125	-0.125		
	0.375	-1.125	0.875		
	0.625	-1.875	1.125		
25	0.625	0.125	0.125	43.8	0.9
	1.625	0.125	0.125		
	0.625	-0.875	1.125		
	2.375	-1.125	0.875		
26	0.625	0.125	0.125	10.5	0.4
	1.625	0.125	0.125		
	1.625	-0.875	0.125		
	1.375	-1.125	1.875		
27	0.625	0.125	0.125	-21.9	-0.9
	1.375	-0.125	-0.125		
	0.625	-0.875	0.125		
	1.375	-0.125	0.875		
28	0.625	0.125	0.125	-20.2	-1.7
	1.625	0.125	0.125		
	1.375	-1.125	0.875		
	1.375	0.875	-1.125		

Sites in Table S1 are based on a $\text{Mg}_2\text{Cr}_4\text{O}_8$ primitive cell with Mg at fractional coordinates (0.375 0.875 0.875) and (0.625 0.125 0.125) in lattice:

$$\begin{pmatrix} 4.16384 & 4.163840 & 0 \\ 4.163840 & 0 & -4.163840 \\ 0 & 4.163840 & -4.163840 \end{pmatrix}$$

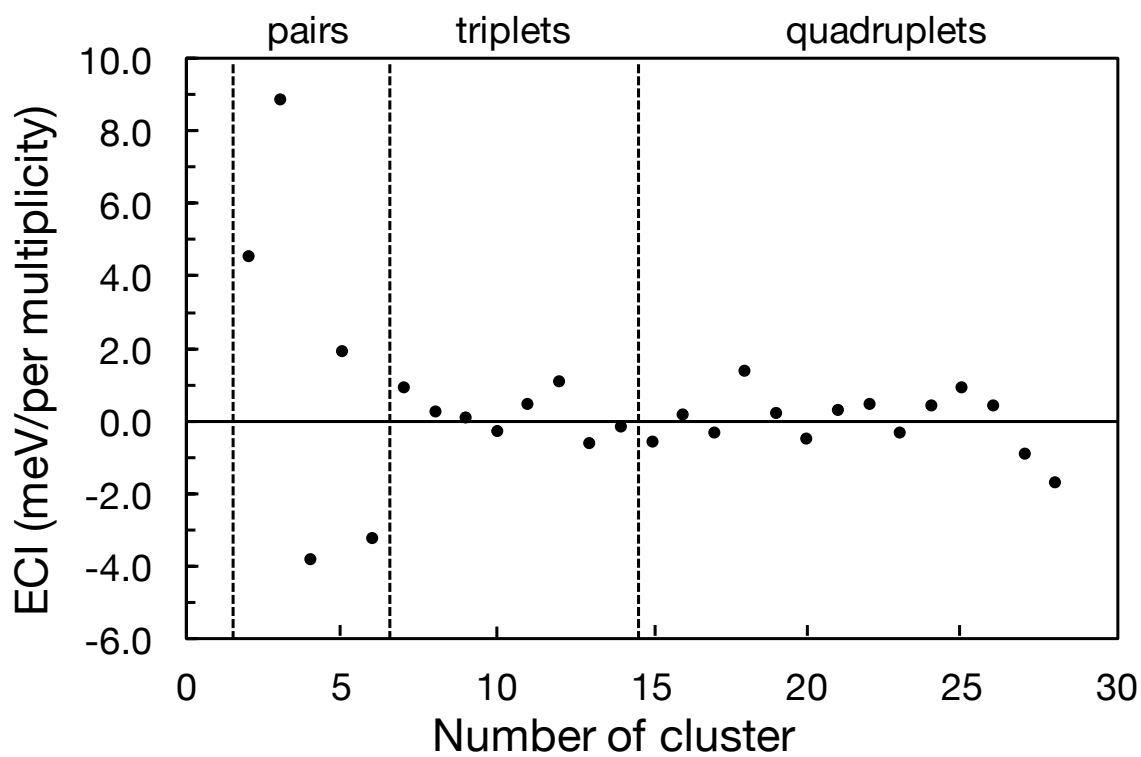


Figure S1: Fitted ECI for formation energy, with cluster number corresponding to clusters in Table S1. The zero- and point-cluster terms are not shown, and the pairs, triplets, and quadruplets ECI's are separated by dashed lines.

1.2 $x = 0.33$ and $x = 0.5$ ground state orderings of $\text{Mg}_x\text{Cr}_2\text{O}_4$

Table S2: Crystallographic information of $x = 0.33$ and $x = 0.5$ ground state orderings of $\text{Mg}_x\text{Cr}_2\text{O}_4$

$\text{Mg}_2\text{Cr}_8\text{O}_{16}$				$\text{Mg}_2\text{Cr}_{12}\text{O}_{24}$			
a	b	c		a	b	c	
5.889	5.889	10.199		5.889	13.167	5.889	
α	β	γ		α	β	γ	
73.221	90.000	120.000		77.079	90.000	77.079	
Cell volume				Cell volume			
288.763				433.145			
Atom	Fractional Coordinates			Atom	Fractional Coordinates		
Mg	0.375	0.75	0.875	Mg	0.916667	0.166667	0.416667
Mg	0.25	0.5	0.25	Mg	0.166667	0.666667	0.166667
Cr	0.5625	0.125	0.3125	Cr	0.375	0.25	0.125
Cr	0.0625	0.125	0.8125	Cr	0.708333	0.583333	0.458333
Cr	0.8125	0.125	0.0625	Cr	0.041667	0.916667	0.791667
Cr	0.3125	0.125	0.5625	Cr	0.708333	0.083333	0.958333
Cr	0.8125	0.625	0.0625	Cr	0.041667	0.416667	0.291667
Cr	0.3125	0.625	0.5625	Cr	0.375	0.75	0.625
Cr	0.3125	0.125	0.0625	Cr	0.375	0.25	0.625
Cr	0.8125	0.125	0.5625	Cr	0.708333	0.583333	0.958333
O	0.94185	0.8837	0.17445	Cr	0.041667	0.916667	0.291667
O	0.44185	0.8837	0.67445	Cr	0.208333	0.083333	0.958333
O	0.18315	0.3663	0.45055	Cr	0.541667	0.416667	0.291667
O	0.68315	0.3663	0.95055	Cr	0.875	0.75	0.625
O	0.67445	0.8837	0.44185	O	0.294567	0.410867	0.527167
O	0.17445	0.8837	0.94185	O	0.6279	0.7442	0.8605
O	0.45055	0.3663	0.18315	O	0.961233	0.077533	0.193833
O	0.95055	0.3663	0.68315	O	0.788767	0.422467	0.056167
O	0.67445	0.3489	0.44185	O	0.1221	0.7558	0.3895
O	0.17445	0.3489	0.94185	O	0.455433	0.089133	0.722833
O	0.45055	0.9011	0.183150	O	0.938033	0.589133	0.705433
O	0.95055	0.9011	0.68315	O	0.271367	0.922467	0.038767
O	0.20925	0.8837	0.44185	O	0.6047	0.2558	0.3721
O	0.70925	0.8837	0.94185	O	0.1453	0.2442	0.8779
O	0.91575	0.3663	0.183150	O	0.478633	0.577533	0.211233
O	0.41575	0.3663	0.68315	O	0.811967	0.910867	0.544567
				O	0.294567	0.410867	0.061967
				O	0.6279	0.7442	0.3953
				O	0.961233	0.077533	0.728633
				O	0.788767	0.422467	0.521367
				O	0.1221	0.7558	0.8547
				O	0.455433	0.089133	0.188033
				O	0.472833	0.589133	0.705433
				O	0.806167	0.922467	0.038767
				O	0.1395	0.2558	0.3721
				O	0.6105	0.2442	0.8779
				O	0.943833	0.577533	0.211233
				O	0.277167	0.910867	0.544567

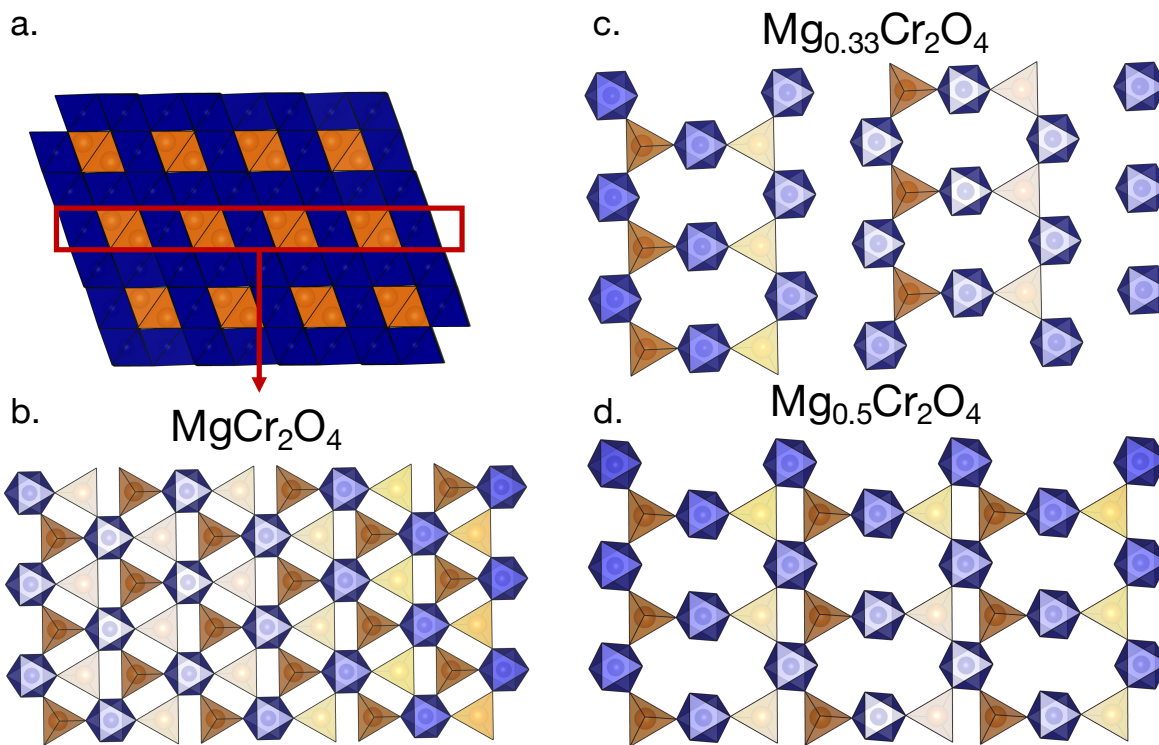


Figure S2: Orderings of Mg in the Mg-Cr layer in various states of Mg concentration x in $\text{Mg}_x\text{Cr}_2\text{O}_4$, with Mg represented by orange tetrahedral and Cr represented by blue octahedral and O at the vertices of the polyhedra. (a) Mg-Cr layer outlined in red in fully magnesiated MgCr_2O_4 . Mg-Cr layer in the (111) direction of (b) MgCr_2O_4 , (c) $\text{Mg}_{0.33}\text{Cr}_2\text{O}_4$, and (d) $\text{Mg}_{0.5}\text{Cr}_2\text{O}_4$.

1.3 Free energy integration

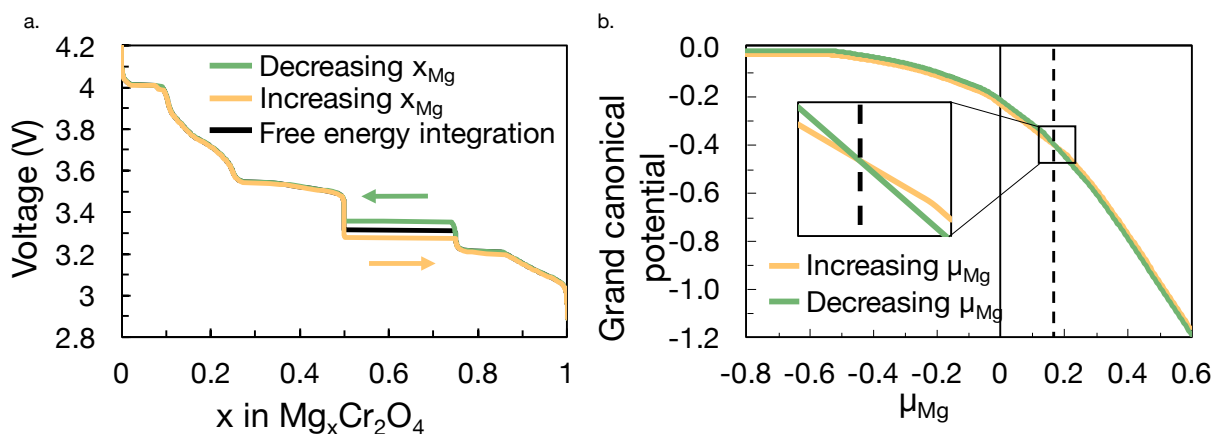


Figure S3: (a) Demonstration of free energy integration from Grand canonical Monte Carlo scans over decreasing x_{Mg} (green) and increasing x_{Mg} (yellow) to obtain the free energy-integrated curve (black). (b) The Grand canonical Monte Carlo scans from (a) plotted in the Grand canonical potential- μ_{Mg} space, with the Grand canonical potential (ϕ) calculated from Equation S1. Yellow and green lines in (b) represent scans in increasing and decreasing μ_{Mg} , respectively. The free-energy-integrated voltage curve in (a) is the lower envelope of the green and yellow lines in (b). The vertical black dashed line marks the μ_{Mg} where the yellow and green lines intersect ($\mu_{\text{Mg}} \sim 1.9$), while the inset shows a zoom-in of the intersection.

Hysteresis can be observed in Monte Carlo simulations, leading to quantitatively different voltage profiles and transition temperatures while simulating phase transitions.¹ For example, from Figure S3a, the voltage curves calculated from an increasing x_{Mg} (yellow line) and a decreasing x_{Mg} (green) Monte Carlo scans differ significantly at $x_{\text{Mg}} \sim 0.5$ (3.27 V in the increasing x_{Mg} scan and 3.36 V in the decreasing x_{Mg} scan). Such hysteresis can be removed via free energy integration. Figure S3 demonstrates free energy integration between $x_{\text{Mg}} \sim 0$ and $x_{\text{Mg}} \sim 1$, which corresponds to $\mu_{\text{Mg}} \sim -0.8$ and $\mu_{\text{Mg}} \sim 0.6$, respectively. The free energy integration is calculated by performing

Grand canonical Monte Carlo scans in both increasing (yellow line in Figure S3b) and decreasing (green) μ_{Mg} and subsequently taking the lower envelope of free energy obtained from the two scans in the Grand canonical potential- μ_{Mg} space. As in Hinuma et al,¹ we calculate the Grand canonical potential at a given μ_{Mg} and temperature ($T = 293$ K) based on the integral of the average concentration $\langle N(T = 293 \text{ K}, \mu) \rangle$ over $d\mu$, from an initial reference state where the Grand canonical potential is known (at $\mu=\mu_0$) as

$$\phi(293\text{K}, \mu_{\text{Mg}}) = \phi(293 \text{ K}, \mu_0) - \int_{\mu_0}^{\mu_{\text{Mg}}} \langle N(293 \text{ K}, \mu) \rangle d\mu . \quad (\text{S1})$$

For the yellow curve in Figure S3b, $\mu_0 \sim -0.8$ ($x_{\text{Mg}} = 0$) and $d\mu > 0$, while the green curve has $\mu_0 \sim 0.6$ ($x_{\text{Mg}} = 1$) and $d\mu < 0$. In Figure S3b, the lower envelope of the yellow and green lines corresponds to the true minimum of the Grand-canonical potential at each μ_{Mg} , i.e., the yellow line from $\mu_{\text{Mg}} \sim -0.8$ to $\mu_{\text{Mg}} \sim 1.9$ and the green line from $\mu_{\text{Mg}} \sim 1.9$ to $\mu_{\text{Mg}} \sim 0.6$, which in turn leads to the voltage curve without any numerical hysteresis (black in Figure S3a). The dashed black line in Figure S3b corresponds to the μ_{Mg} at which the green and yellow line intersect in the Grand canonical potential- μ_{Mg} space (Figure S3b). After free energy integration, the voltage plateau from $x_{\text{Mg}} \sim 0.5$ to $x_{\text{Mg}} \sim 0.75$ is 3.31 V.

From Figure S3a (black), we note that we are missing a 33% Mg voltage step in the free energy-integrated voltage curve. However, we consider the 33% Mg ground state to be important due to its high depth (Figure 3 in main text). Further, canonical Monte Carlo scans (at constant x_{Mg}) and increasing temperature indicate that the 33% Mg structure should be a ground state at both 0 K and 293 K. Thus, to obtain an accurate voltage curve including the 33% Mg ground state, we use

a free energy integration scheme between 25% and 50% Mg and initiate Monte Carlo scans from the missing 33% Mg configuration.

Figure S4 demonstrates free energy integration between 25% and 50% Mg ($\mu_{\text{Mg}} \sim -0.3$ to $\mu_{\text{Mg}} \sim 0.2$), analogous to Figure S3. Here, we start from the free energy-integrated curve of Figure S3 (also black in Figure S4a-b) and perform Grand canonical Monte Carlo scans from an initial $\mu_0 = 0$ ($x_{\text{Mg}} \sim 33\%$, the ground state at 293 K) with, separately, increasing (yellow in Figure S4b) and decreasing (green) μ_{Mg} . The voltage curve from the free energy integration (red curve in Figure S4a) is given by the lower envelope of the yellow, green, and black curves in Figure S4b, which is composed of the black curve from $\mu_{\text{Mg}} \sim -0.3$ to $\mu_{\text{Mg}} \sim -0.15$, the green curve from $\mu_{\text{Mg}} \sim -0.15$ to $\mu_{\text{Mg}} \sim 0$, the yellow curve from $\mu_{\text{Mg}} \sim 0$ to $\mu_{\text{Mg}} \sim 0.07$, and the black curve from $\mu_{\text{Mg}} \sim 0.07$ to $\mu_{\text{Mg}} \sim 0.2$. Thus, the configurations along the lower envelope of Figure S4b are $\sim 25\%$ Mg from $\mu_{\text{Mg}} \sim -0.3$ to $\mu_{\text{Mg}} \sim -0.15$, 33% Mg from $\mu_{\text{Mg}} \sim -0.15$ to $\mu_{\text{Mg}} \sim 0.07$, and 50% Mg from $\mu_{\text{Mg}} \sim 0.07$ to $\mu_{\text{Mg}} \sim 0.17$. The voltage curve in Figure S4a exhibits a voltage jump at 33% Mg from 3.46 V to 3.66 V due to the second free energy integration we perform between 25% Mg and 50% Mg.

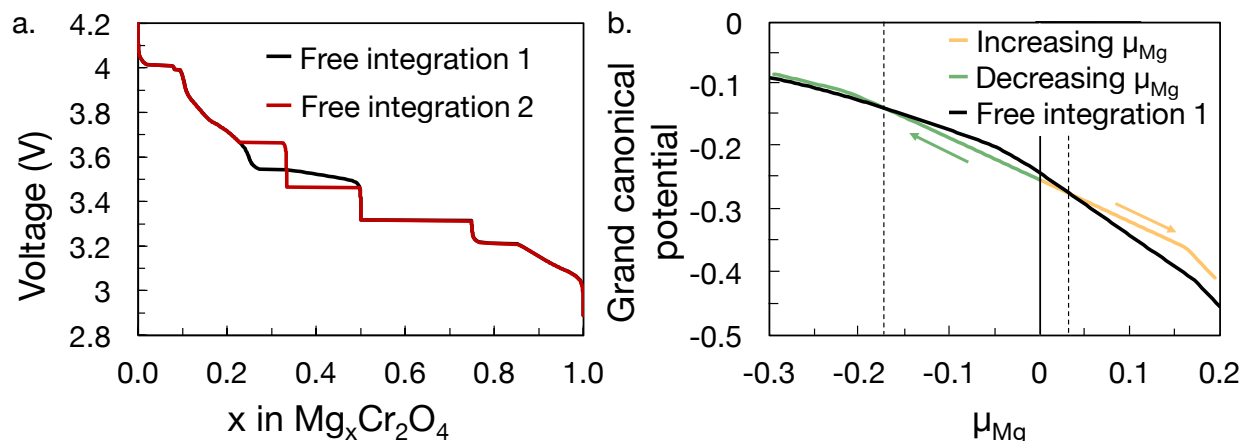


Figure S4: (a) Plot of the voltage curve before (black) and after (red) free energy integration to obtain a voltage curve with the 33% Mg voltage step starting from the voltage profile obtained over the entire Mg composition range obtained in Figure S3 (black line in Figure S3). (b) Grand canonical Monte Carlo scans starting from $\mu_0 = 0$ and increasing (yellow) and decreasing (green) in μ_{Mg} . We additionally show the curve from the first free energy integration (from Figure S3) in the Grand chemical potential- μ_{Mg} space (panel b). The red curve in (a) is obtained by taking the lower envelope of the yellow, green, and black curves in (b). The vertical dashed black lines in (b) show where the green and black curves intersect ($\mu_{\text{Mg}} \sim -1.5$) and where the yellow and black curves intersect ($\mu_{\text{Mg}} \sim 0.07$).

1.4 Volume change during Mg intercalation

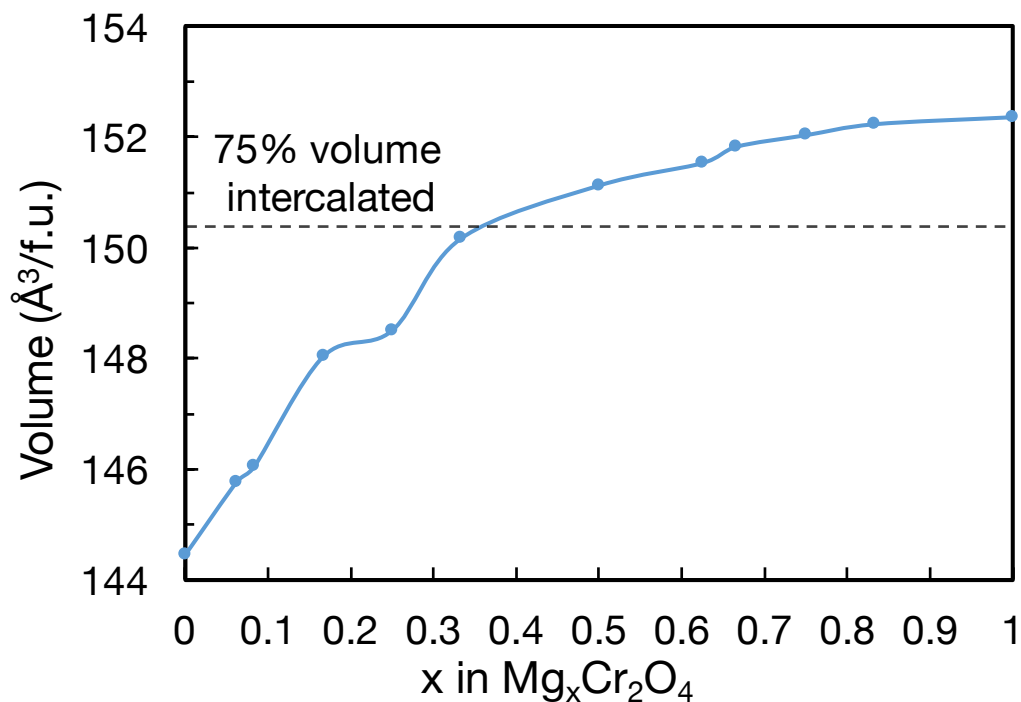


Figure S5: Volume expansion of $\text{Mg}_x\text{Cr}_2\text{O}_4$ ground states as Mg is intercalated from the system is shown through a plot of the volume/f.u. of the DFT ground states against the Mg concentration. The dashed line indicates where 75% of the volume increase occurs during Mg intercalation into the charged- Cr_2O_4 .

Figure S5 plots the volume/f.u. of the ground states at the corresponding Mg concentrations of the ground states to investigate the volume change during intercalation. From the fully charged to the fully discharged states, the structure experiences a total volume expansion of 5.2%. Interestingly, the spinel lattice expands most rapidly at low levels of magnesianation, leading to a 4.0% volume increase from the 0% Mg (at $144.5 \text{ \AA}^3/\text{f.u.}$) to the 33% Mg (at $150.2 \text{ \AA}^3/\text{f.u.}$). Beyond 33% Mg, the spinel expands to a lesser extent, further increasing 1.5% in volume (up to $152.4 \text{ \AA}^3/\text{f.u.}$) at 100% Mg. Thus, 72.5% of the total volume expansion occurs between 0% Mg and 33% Mg while the remaining 27.5% of the total volume expansion occurs between 33% Mg and 100% Mg content.

1.5 Calculated voltage curves

Figure S6 plots the 333 K voltage curve calculated from Monte-Carlo simulations of the CE (solid blue). Note that the 333 K voltage curve lies directly on top of the 293 K CE-predicted voltage curve (solid black line), indicating that there should be negligible change in the voltage profile with the increase in temperature from 293 K to 333 K.

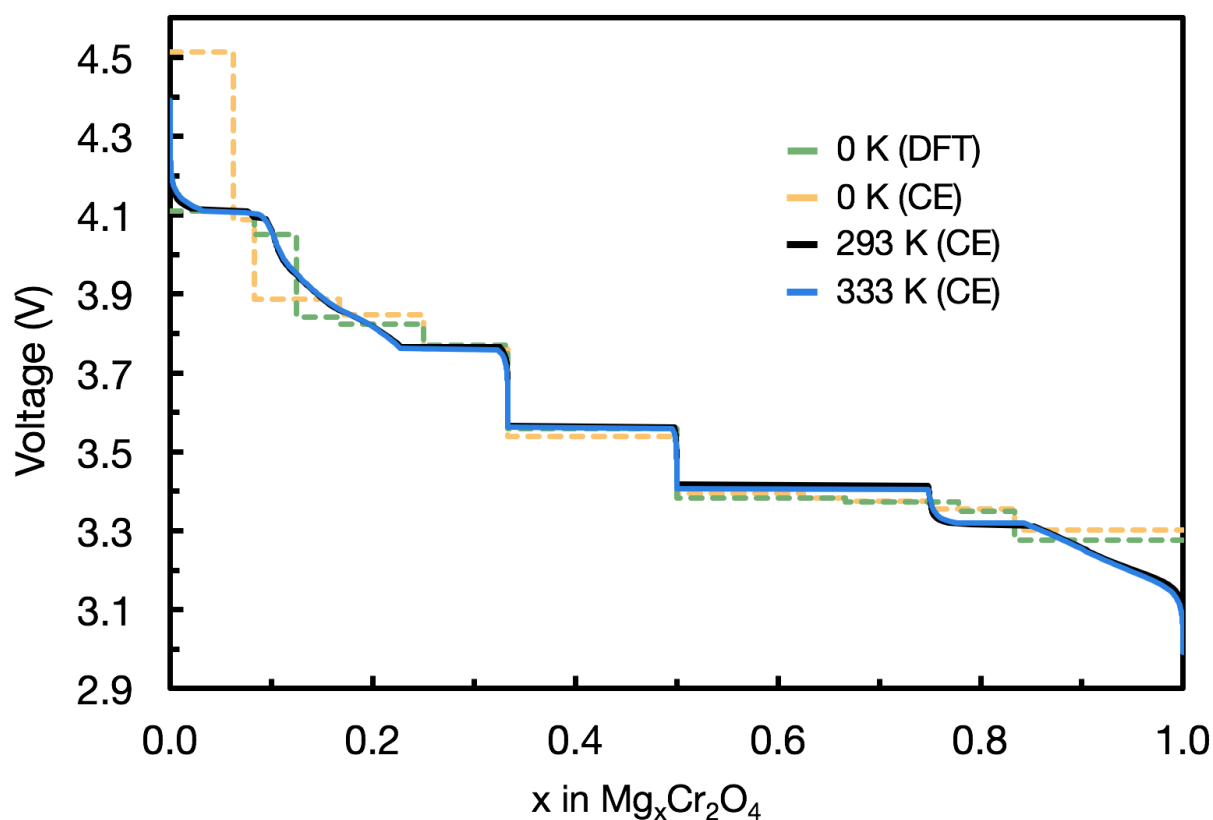


Figure S6: Voltage curves calculated from the DFT convex hull (green dashed), from the CE-predicted convex hull at 0 K (yellow dashed), from Monte Carlo calculations using the CE at room temperature (293 K, black), and from Monte Carlo calculations using the CE at 60° (333 K, blue).

1.6 Migration path of additional Mg in $\text{Mg}_{0.5}\text{Cr}_2\text{O}_4$ ground state ordering

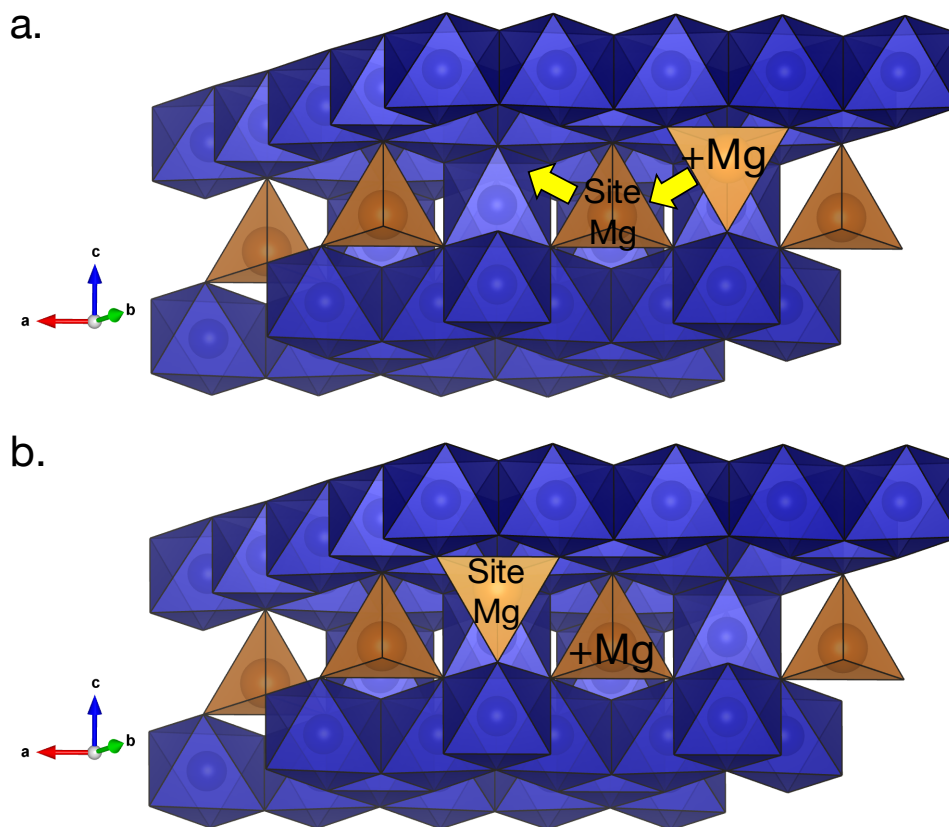


Figure S7: (a) Initial and (b) final states of the considered migration path for the 50% Mg with additional Mg configuration. The added Mg, labeled '+Mg', is inserted in a site that is not occupied in the 50% Mg ground state ordering. '+Mg' migrates to an adjacent Mg site which is occupied in the 50% Mg ground state ordering, labeled 'Site Mg'. Because the adjacent site is occupied in (a) by 'Site Mg', the migration of '+Mg' from inserted site to adjacent site is accompanied by the migration of 'Site Mg' from the adjacent site to a site equivalent to the inserted site.

1.7 Comparison between GGA+ U and GGA NEB barriers

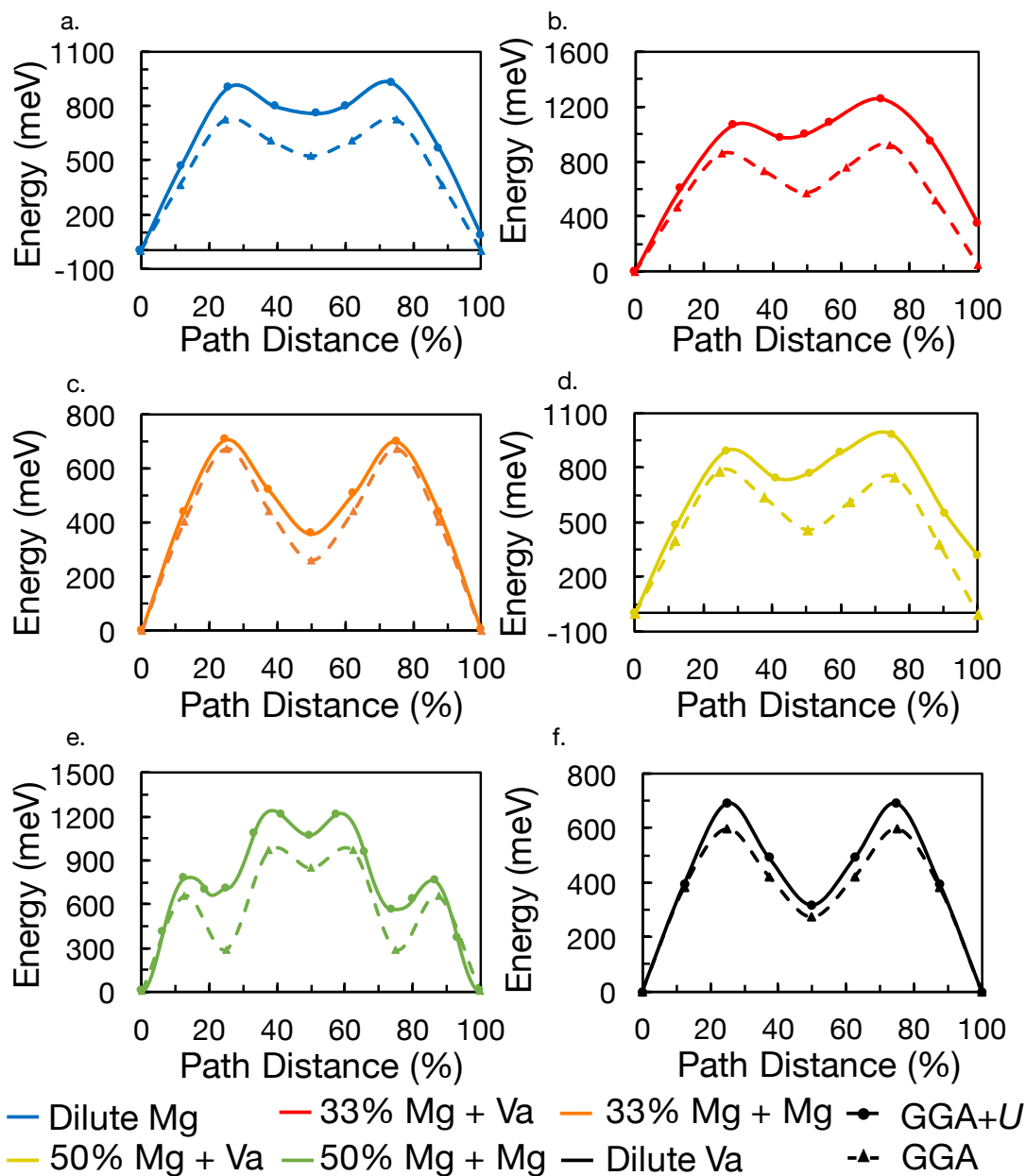


Figure S8: Comparison between the activation migration barriers using the GGA (dashed) vs. GGA+ U (solid) functionals in DFT-based NEB. The migration barriers are shown at the dilute Mg (blue), 33% Mg with additional vacancy (red), 33% Mg with additional Mg (orange), 50% Mg with additional vacancy (yellow), 50% Mg with additional Mg (green), and dilute vacancy (black) configurations.

Figure S8 shows in each plot a comparison between the migration barriers calculated using DFT with GGA (solid) and GGA+ U (solid). Migration barriers were calculated for the dilute Mg, 33% Mg (with both additional vacancy and additional Mg), 50% Mg (with both additional vacancy and additional Mg), and dilute vacancy configurations (see Figures 6 and 7 in main text). In all cases, the GGA+ U barriers are higher than the GGA barriers for the same configuration. The dilute Va and 33% Mg with additional Mg barriers are the most similar between GGA and GGA+ U , with a barrier increases of only ~ 90 meV and ~ 30 meV respectively with GGA+ U compared to the GGA barrier. However, the barriers of the dilute vacancy, 33% Mg with additional Mg, 50% Mg with additional vacancy, and 50% Mg with additional Mg configurations increase considerably, by ~ 200 meV, ~ 320 meV, ~ 200 meV, and ~ 250 meV respectively, when GGA+ U is employed instead of GGA. Also, the migration energy profiles at 33% Mg and 50% Mg with additional vacancies demonstrate a large difference in energy (300-350 meV) between the initial site (0% path distance) and final site (100% path distance) when using GGA+ U instead of GGA.

1.8 Comparison of convex ground state hulls of $\text{Mg}_x\text{Cr}_2\text{O}_4$ using GGA vs. GGA+ U functionals

Figure S9 shows a comparison between the convex hulls of the $\text{Mg}_x\text{Cr}_2\text{O}_4$ when calculating energies of configurations using DFT using the GGA vs. GGA+ U functionals. In order to demonstrate the difference in functionals, we consider only the GGA+ U ground states when calculating both of the convex hulls. Notably, 8.3%, 25%, 62.5%, and 75% ground states in GGA+ U are no longer ground states when the energies are calculated using GGA. Further, the 16% Mg and 66% Mg ground states are much deeper (from $E_{\text{tie-line}} < 5 \text{ meV}$ to $E_{\text{tie-line}} > 10 \text{ meV}$). Thus, both the shape of the ground state hulls (which affects the voltage) and the depths of ground state configurations (which indicate the important Mg-Va orderings that may lead to high Mg migration barriers) are evaluated differently in GGA compared to GGA+ U .

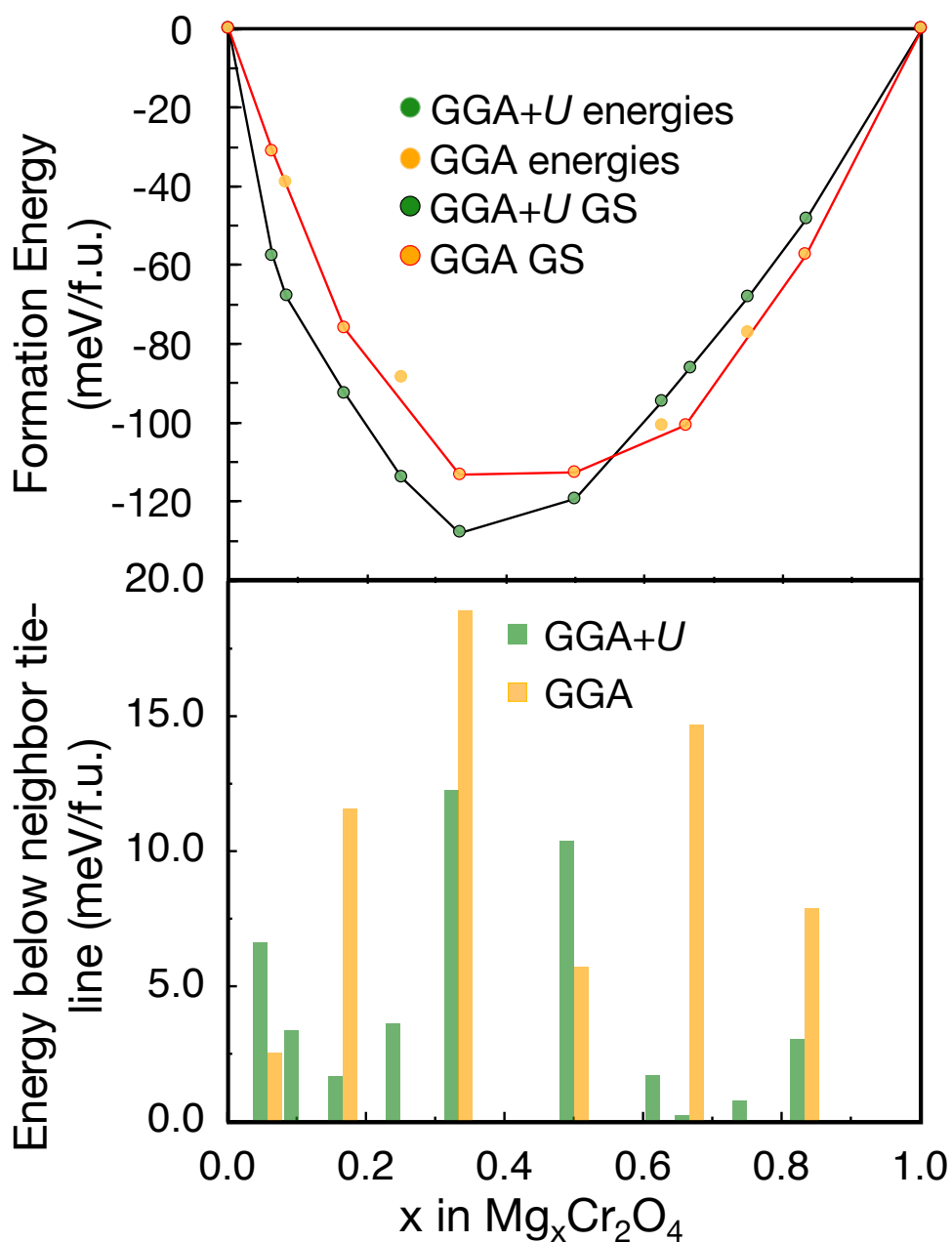


Figure S9: Comparison between the convex hulls of the $\text{Mg}_x\text{Cr}_2\text{O}_4$ system with configurations calculated in DFT using the GGA (yellow circles) vs. GGA+U (green circles) functionals. The GGA+U convex hull is delineated in black (with ground states outlined in black), while the GGA convex hull is delineated in red (and ground states outlined in red). The GGA convex hull was constructed by calculating the energies of the GGA+U ground states within the GGA framework.

References

1. Hinuma, Y.; Meng, Y. S.; Ceder, G., Temperature-concentration phase diagram of $P2\text{-Na}_x\text{CoO}_2$ from first-principles. *Physical Review B* **2008**, *77*, (22), 224111-224111.